

By acceptance of this article, the publisher or recipient acknowledges the U.S. Government's right to retain a nonexclusive, royalty-free license in and to any copyright covering the article.

MFTF- α +T END PLUG MAGNET DESIGN*

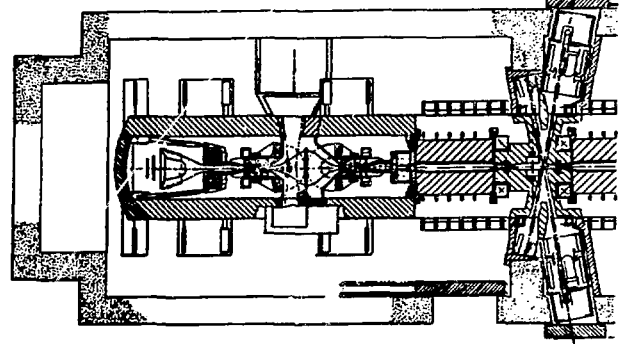
Vishnu C. Srivastava and Joseph A. O'Toole
General Electric Company/Grumman Aerospace Corporation
Fusion Engineering Design Center
Oak Ridge National Laboratory
Oak Ridge, Tennessee 37831

Abstract: The conceptual design of the end-plug magnets for MFTF- α +T is described. MFTF- α +T is a near-term upgrade of MFTF-B, which features new end plugs to improve performance. The Fusion Engineering Design Center has performed the engineering design of MFTF- α +T under the overall direction of Lawrence Livermore National Laboratory. Each end plug consists of two Yin-Yang pairs, each with $\sim 2.5:1$ mirror ratio and ~ 5 -T peak field on axis; two transition coils; and a recircularizing solenoid. This paper describes the end-plug magnet system functional requirements and presents a conceptual design that meets them. The peak field at the windings of the end-plug coils is ~ 6 T. These coils are designed using the NbTi MFTF-B conductor and cooled by a 4.2K liquid helium bath. All the end-plug magnets are designed to operate in the cryostable mode with adequate quench protection for safety. Shielding requirements are stated and a summary of heat loads is provided. Field and force calculations are discussed. The field on axis is shown to meet the functional requirements. Force resultants are reported in terms of winding running loads and resultant coil forces are also given. The magnet structural support is described. A trade study to determine the optimum end-cell coil internal nuclear shield thickness and the resulting coil size based on minimizing the end-cell life cycle cost is summarized.

a 2.5:1 mirror ratio for thermal barrier function. In addition, the magnetic field contours must not cause MHD instability.

The plasma leaving the end-plug region must be nearly circular to simplify the design of the direct converter. The magnet dimensions and locations must be compatible with several system integration constraints, including the space required for drift pumps, sloshing beams, and ICRH and ECRH subsystems. The magnets must have sufficient clear bore to accommodate the plasma with its halo and the internal magnet shielding. The resulting axial field profile and the magnet configuration that satisfies these requirements are shown in Fig. 2.

ORNL-DWG 83-4018 FED



Introduction

A three-dimensional view of the magnet system for MFTF- α +T is shown in Fig. 1, which also identifies the magnets to be taken from the existing MFTF-B device.

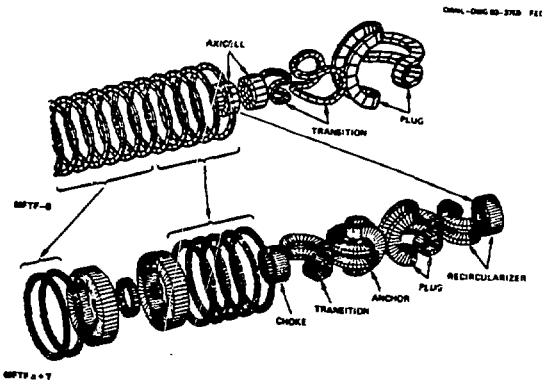


Fig. 1. Coil configuration for MFTF-B and MFTF- α +T.

The magnet system for MFTF- α +T is described in detail in Ref. 1. The c-shaped (Yin-Yang) coils in MFTF- α +T are approximately one-third the size of the Yin-Yang magnets for MFTF-B.

Requirements and Configurational Constraints

The axial field requirements are that the end-cell magnets (transition, anchor, plug, recircularizer coils) must provide ~ 5 -T peak field on axis and have

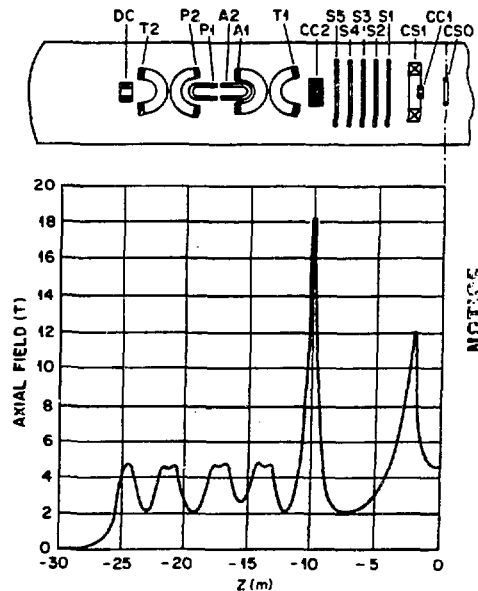


Fig. 2. Magnet System Configuration and the resulting Axial Field Profile.

End-Cell Magnet Design

All the end-cell magnets are new except for the recircularizing solenoid coil, which can be taken from MFTF-B. The peak field at the windings of the c-shaped coils is ~ 6 T. These coils use NbTi MFTF-B conductor with liquid helium (LHe) bath cooling (4.2K) and operate in a cryostable mode.

DISTRIBUTION OF THIS DOCUMENT IS UNLIMITED

NOTICE
PORTIONS OF THIS REPORT ARE AVAILABLE.
It has been reproduced from the best available copy to permit the broadest possible availability.

MASTER

* Research sponsored by the Office of Fusion Energy, U.S. Department of Energy, under contract W-7405-eng-26 with the Union Carbide Corporation.

DISCLAIMER

This report was prepared as an account of work sponsored by an agency of the United States Government. Neither the United States Government nor any agency thereof, nor any of their employees, makes any warranty, express or implied, or assumes any legal liability or responsibility for the accuracy, completeness, or usefulness of any information, apparatus, product, or process disclosed, or represents that its use would not infringe privately owned rights. Reference herein to any specific commercial product, process, or service by trade name, trademark, manufacturer, or otherwise does not necessarily constitute or imply its endorsement, recommendation, or favoring by the United States Government or any agency thereof. The views and opinions of authors expressed herein do not necessarily state or reflect those of the United States Government or any agency thereof.

Conductor Description and Operating Current

The MFTF-B conductor shown in Fig. 3 has been chosen for the end-cell c-shaped coils. The conductor [2] has been successfully fabricated, tested, and operated in the Yin-Yang coils of MFTF-B, giving a high degree of confidence to its use for a similar application in MFTF- α T. Its key parameters are given in Table 1.

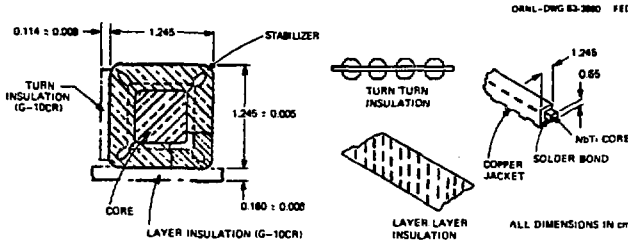


Fig. 3. MFTF-B Conductor for the c-shaped coils.

Table 1. NbTi Conductor parameters for end plug magnets

Parameter	Grade I	Grade II
Composite size (mm)	6.5 × 6.5	6.5 × 6.5
Composite RRR	150	150
Filament diameter (mm)	0.20	0.20
Number of filaments	480	480
Twist pitch (mm)	180	180
Composite Cu/SC ratio	1.7:1	6.0:1
Conductor size (mm)	12.4 × 12.4	12.4 × 12.4
Stabilizer RRR	220	220
Overall Cu/SC ratio	6.7	18.7
Total copper area	1.07	1.17
Wetted area (cm ² /cm)	8.17	7.940
Critical current at 4.5 K (kA)	12.5 (6 T)	7.2 (5.1 T)

The critical current as a function of field and the magnet load line are shown in Fig. 4. A 5-kA operating current was chosen based on static stability, margin against critical current, and helium bubble ventilation considerations. The operating current is limited by heat transfer rather than by critical current, as the peak field on the windings is ~6 T.

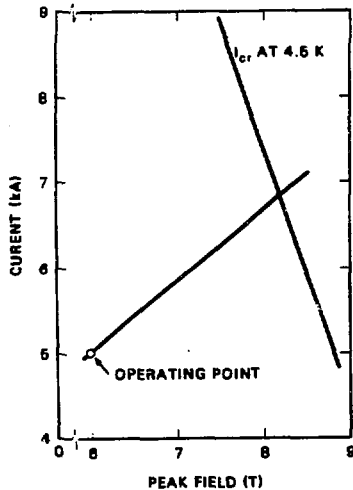


Fig. 4. Critical Current of Grade I Conductor as a function of field and magnet loadline for c-shaped coils.

Winding Layout

The winding layout for all the c-shaped coils is shown in Fig. 5; their main parameters are listed in Table 2.

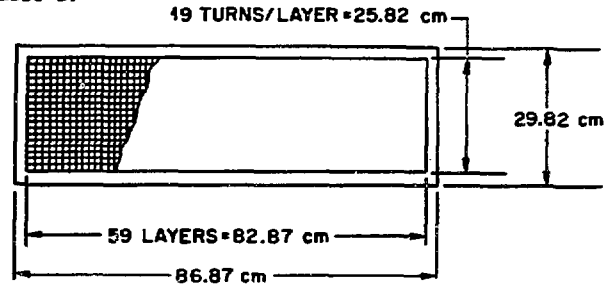


Fig. 5. C-shaped Coils Winding Layout.

Table 2. Main parameters of end plug magnets

Coil	Axial Location, m	Diameter (solenoids) or Major/Minor radii (Coc Coils), m	Sweep Angle, Deg. Coc Coils)	Coil Current, MAT	Winding Dimensions S1/S2, m	Winding Current Density A/cm ²	Energy (kJ)
T1	±11.811	1.5/0.5	80	5.6	0.869/0.298	2162	61
A1	±15.611	1.3/0.5	90	5.6	0.869/0.298	2162	62
A2	±15.611	1.3/0.5	90	5.6	0.869/0.298	2162	62
P1	±19.411	1.5/0.5	80	5.6	0.869/0.298	2162	60
P2	±19.411	1.5/0.5	80	5.6	0.869/0.298	2162	60
T2	±23.211	1.3/0.5	71	5.6	0.869/0.298	2162	45
DC	±24.711	1.856	—	9.2	0.94/0.41	1900	52

The 5-kA operating current is 73% of the critical current along the magnet load line. Each winding is layer wound like the MFTF-B Yin-Yang coils. Each of the c-shaped coils provides 5.6 MAT using 1121 turns. The winding is graded to minimize cost; grade I conductor is used for peak fields ≥ 5 T; grade II conductor, for fields < 5 T. The turn-to-turn and layer-to-layer insulation concept is identical to that used for the MFTF-B Yin-Yang coils. The integrated lifetime dose in these coils will be ~10¹⁰ rad. Polyimide is specified as the insulation material. This reduces the overall end-cell system cost by permitting a thinner internal nuclear shield, which reduces the size of the coil set and its surrounding shield and vessel.

Performance Analysis

Static Stability and Winding Performance

The windings of the c-shaped coils are cooled with a pool boiling LHe bath at ~4.2K. The 5 kA operating current was chosen based on a static stability analysis. Heat deposited in a short normal zone by resistive loss, neutronic heating, and heat transfer from the coil case was calculated.

Table 3. Peak heat loads and stability considerations

Parameter description	Winding	Coil case contribution	Total
Peak heat loads in grade I conductor (W/cm)			
Nuclear heating	0.01	0.04	0.05
Joule heating in normal zone	1.16	0	1.16
Total peak heat load	1.17	0.04	1.21
Peak heat flux at the conductor surface (W/cm ²)			0.15
Critical recovery heat flux (W/cm ²)			9.19

From this result, the peak surface heat flux required to remove the total heat load was computed (see Table 3). The design of the coil set and its internal nuclear shield limits the peak surface heat flux to 80% of the critical recovery heat flux for the conductor (0.19 W/cm²). It was found that the permissible operating current consistent with the critical heat recovery flux is not significantly affected by neutronic heating nor, therefore, by the shield thickness. With only the shielding provided by the coil case, the operating current can be 5 kA. At the other extreme, with an infinitely thick shield, so that there is no neutronic heating, the operating current is 5.25 kA. Therefore, the operating current was set at 5 kA for the c-shaped coils, ensuring local cryostability, even with no shielding. The resulting penalty in the operating current density is small, and this choice of current ensures that streaming paths or local thinning of shield will not compromise the local cryostability of the winding, as long as adequate helium bubble clearance is provided.

Helium Bubble Clearance

Individual LHe supply dewars for each of the c-shaped coils will be located on top of the vacuum vessel for enhancing bubble clearance through the winding [2, 3]. These dewars will supply LHe to the bottom of each magnet; the return flow will be from the top of each magnet to its dewar above. LHe cooling of a conductor is inhibited when it is bathed in vapor instead of liquid. To ensure cryostability, a minimum helium quality of 2.5 wt % (~14 vol %) has been specified. LHe in the inlet dewar is assumed to be at 4.35 K and at the saturation pressure. Because of static head, the LHe is subcooled at the inlet, receives heat as it passes through the magnet, and exits at the top of the coil. The exit conditions depend upon the heat loads in the coil. However, because of heating, the helium exiting the coil is less dense than the supply helium. The difference in density between the supply and return lines produces a finite pressure difference and a net flow of LHe through the winding.

Thermal-hydraulic analysis of a typical c-shaped coil and its helium dewar supply system was performed to determine system flow rates and exit quality of the coolant [3,4]. Vapor content by volume as a function of integrated heat load is shown in Fig. 6.

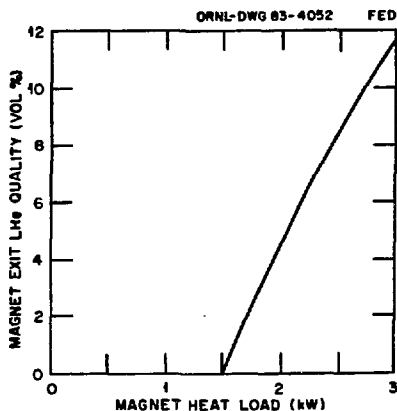


Fig. 6. Quality of LHe leaving a coil as a function of heat load.

As may be seen, subcooling of helium permits a heat load of 1.5 kW before boiling is initiated. Vapor content increases with increasing heat load, with 10% vapor by volume being reached at a heat load of 2.7 kW.

The calculations described above also provide the important result that the helium flow velocity through the magnet, due to the difference in density between the supply and return lines, is large compared to the free rise velocity of vapor bubbles in LHe. For example, for a 2-kW heat load, the mass velocity flow through the magnet is 34 cm/s, compared to a free bubble rise velocity of 2 cm/s. Thus, bubbles will be swept out by the bulk helium flow and not percolate through the winding to pocket on the upper surface of the case. The windings are thus expected to operate in the cryostable mode.

Quench Analysis

The discharge voltage and the hot spot temperature in the winding are limited to 1000 V and 200K, respectively. Discharge data have been computed using the Thermal Analysis for Stability and Safety (TASS) code [5] for pool boiling magnets. The discharge characteristics, with an external 0.17-Ω dump resistor, are shown in Fig. 7. This meets the design requirements.

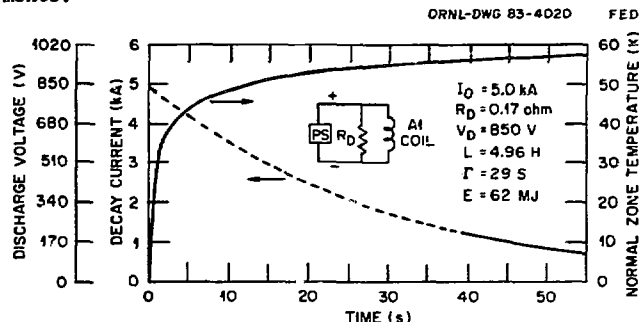


Fig. 7. Quench characteristics of typical c-shaped coil (anchor A1).

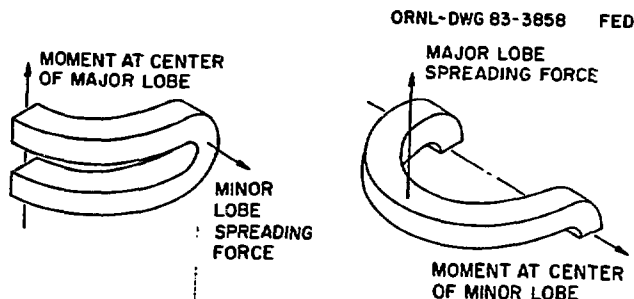
Magnetic Loads and Winding Pack Stresses

Magnetic forces on the coils were computed using the EFFI code, with the coils modeled as a series of circular arcs with finite uniform current density. Magnetic loads on the end-cell magnets are summarized in Table 4.

Table 4. Summary of magnetic loads on the end cell coils

Coil	Maximum running load, MN/m		Lobe spreading forces, MN		Axial force, MN
	In-plane	Out-of-plane	Major lobe	Minor lobe	
T1	5.60/11.48 ^a	10.06/4.028 ^a	46.4	13.1	3.018
A1	5.783/13.29	11.18/2.280	52.4	10.0	4.482
P1	5.594/11.31	10.30/2.077	52.5	10.0	-1.943
P2	5.435/11.44	9.899/2.048	47.4	11.1	1.013
T2	6.033/11.13	9.660/3.016	37.5	12.8	-3.741
BC	22.03	-1.260			-6.968

^aMajor lobe/minor lobe.



Out-of-plane running loads accumulate from turn to turn and are transmitted in bearing to the coil case. In-plane loads are equilibrated by hoop membrane stress in each turn. The bearing stress and hoop stress in the conductor are computed as

$$\sigma_{brg} = f_o/N_L h, \quad \sigma_\theta = f_i R_m/NA \quad (\text{major lobe}),$$

$$\sigma_{brg} = f_o/N_T h, \quad \sigma_\theta = f_i R_m/NA \quad (\text{minor lobe}),$$

and compared with the allowable primary membrane stress of 159 MPa (23 ksi) in quarter-hard copper. In the equations for conductor stress f_o and f_i are the running loads given in Table 4; R_m and R_m are the major and minor radii, respectively; N_L , N_T , and $N = N_T N_L$ are the number of layers, number of turns/layer, and total number of turns; h is the height of the conductor; and A is the conductor cross-sectional copper area. The maximum bearing stress has been calculated to be 17.0 MPa and occurs in the minor lobe of coil A2. The maximum hoop stress is 70.6 MPa and occurs in the major lobe of coil T1. These stresses are less than the allowable of 159 MPa (23 ksi). The actual hoop stress will be less than that conservatively calculated due to the action of the coil support structure.

Coil Support Structure Design

Each c-shaped coil has a structural case made of 316 LN stainless steel that supports the magnet winding and contains the liquid helium coolant. Each coil's minor lobe opening force is supported by its structural case. Two types of support are used for the coil's major lobe opening force. The first type, a strong-back and tension-tie structure, is used for the two transition coils. The second type is used for each of the Yin-Yang pairs, the anchor and plug coil sets. This structure consists of four identical collar assemblies, as shown in Fig. 8.

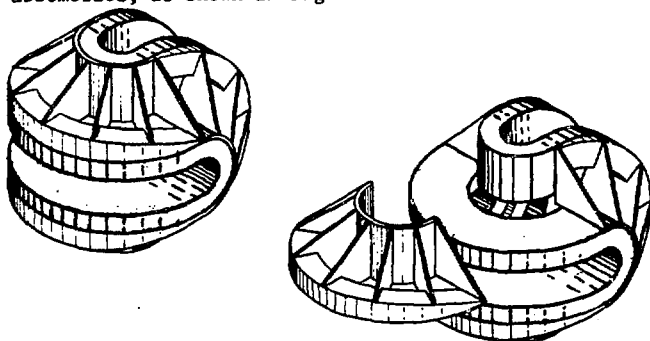


Fig. 8. Anchor and plug coil support structure.

The plug coils have a sweep angle of 80° , which requires them to have a short flat built into the side of the minor radius area of the case so that all four collars are identical. Each coil of the pair acts as a C-clamp to support the greater part of its mate's major lobe opening force.

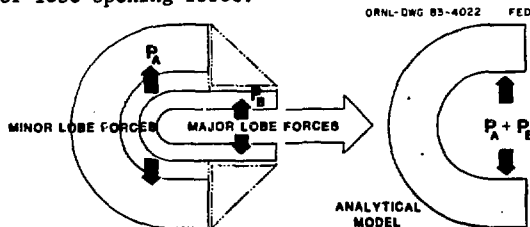


Fig. 9. Concept for supporting the anchor and plug coil forces.

Thus the critical section through each coil's case, which is located midway along its major lobe, is subjected to the axial load and bending moment of the sum of the coil's minor lobe opening force (P_A) and the other coil's major lobe opening force (P_B), as shown in Fig. 9.

Structural analysis of the c-shaped coil support structure was limited to demonstrate feasibility. The transition coil strong-back concept was compared to the MFTF-B A-cell coil structure, which was analyzed in some detail, including the use of a finite element model. The major lobe spreading force on the T1 coil is 46.4×10^6 N; for T2, 37.5×10^6 N. On the A-cell coil design, the strong back supports a load of 127.6 $\times 10^6$ N (10.3×10^6 lb) and has a total span of 7.62 m (300 in.). The T1 coil strong-back has a total span of approximately 3.4 m. It was concluded that with a similar load but a span less than half that of the A-cell design, a structure similar to the A-cell strong-back could have a smaller depth and still prove feasible. Thus, the concept drawings show a strong-back-type structure. For the A-cell design, a minor radius superstructure was necessary to prevent part of the spreading load from entering the minor radius region of the coil. The transition coil support concept does not need a superstructure due to the combined effects of two differences in the coil geometries. One, the transition coil half-angle is 80° , while the A-cell coil has a much smaller half-angle. Two, the total span of the transition coil strong-back is less than half that of the A-cell coil strong-back. The effect of the first is to move the minor radius region out of the central region, thus decreasing its stiffness relative to the strong-back in regard to major lobe spreading force support. The effect of the second is to greatly increase the stiffness of the strong-back. It is anticipated that an analysis of the total support system will show that these two effects will make minor radius clamping unnecessary for the transition coils.

Structural analysis for the anchor and plug coil sets was limited to sizing the coil case and support structure at the critical cross section midway along the major lobe. With a stress limit of 50 ksi for combined tension and bending stress, the cross section required was determined. The material needed at the outer ring proved too thick and interfered with the adjacent coil structure. The space between coil winding cavities is used to adjust for MHD equilibrium of the magnetic configuration and cannot easily be changed. It was, therefore, necessary to configure the coil case structure as shown in Fig. 8 by adding a boxlike outer beam cap structure to the collars. The coil case supports the coil minor lobe opening force, P_A and its bending moment. The complementary coil major lobe opening force P_B and its bending moment are supported by the collar structure and the coil case. The major lobe opening forces are introduced into the case structure as shown in Fig. 9. The moment is introduced by a compression load at the outer region of the coil minor radius. This load is carried in bulk compression through a set of wedges used to accommodate manufacturing tolerances, including radius mismatch, and ensure a tight fit. The complementary tension load is carried through the first collar structure into the second collar structure. This tension load could be carried through a welded or bolted connection. The second collar introduces the load into the coil through bulk compression of a set of wedges located along two areas of each of the two coil major lobes. The wedges accommodate manufacturing tolerances and ensure a tight fit.

The two coils that make up a set are assembled by locating them with respect to each other and then by installing the collar structures. Finally the wedges

are installed. If necessary, the design can accommodate a shim over the major lobe surface of the coils to allow for manufacturing tolerances. This shim could be accomplished by the use of a bladder constructed of thin stainless steel sheets and injected to conform to the coil case structure to collar structure gaps. This bladder design would be similar to that used for the MFTF-B Yin-Yang coil set. This system will allow alignment of the coils into a coil set with the proper magnetic geometry.

End Cell Magnet Shield Thickness and System Cost Trade Study

A trade study was performed to determine the thickness of the shield between the end-cell c-shaped coils and the plasma. The thicker the shield, the greater the capital cost of the end-cell magnets, vacuum vessel and external shield. On the other hand, the capital cost of the cryoplant and the operating cost of cooling the coils decrease as shield thickness increases. The study was undertaken to determine the thickness that would minimize life cycle cost. A functional constraint on the optimization is that the integrated heat load on a coil must produce no more than 10% vapor by volume at the exit of the LHe from the coil.

The end-cell c-shaped coil parameters used for this trade study were given in Table 2 with the exception that the winding dimensions were 0.2 by 0.3-m with winding current density of 3473 A/cm². From a configuration drawing completed for this winding geometry, it was determined that nominally 15 cm of water-cooled stainless steel shielding could be accommodated after allowing for the coil case, clearances, cold wall, drift pump coils, the plasma, and its halo. System life cycle cost was calculated as a function of shield thickness. Operating costs were based on a 10-year life and a 10% duty factor. System cost as a function of shield thickness is shown in Fig. 10.

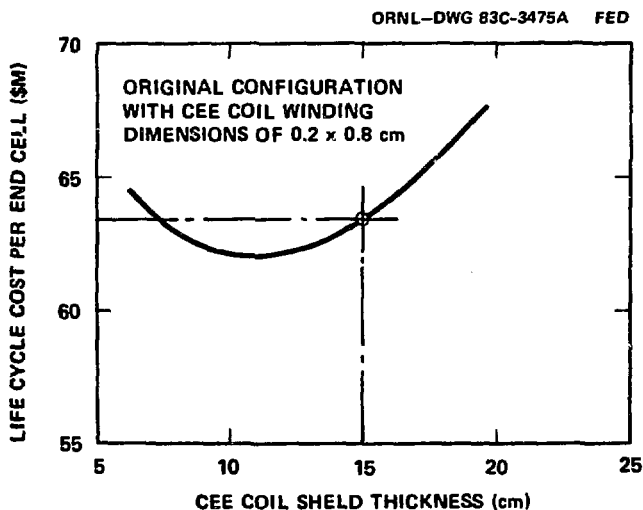


Fig. 10. End cell magnet system cost dependence on the c-shaped coils' internal shield thickness.

As discussed earlier, a 5-kA operating current was selected for the c-shaped coils. For this current, the 0.2- by 0.8-m winding space for the coils was found to be insufficient to provide the required MA-turns. A new baseline was defined with a winding cavity of 0.30 by 0.87-m, with no change in coil centerline dimensions (major and minor radii). The revised winding size

impact on system cost and machine size. The long dimension of the winding was increased as much as deemed prudent without necessitating an increase in the spacing between the coils along the axis of the machine. With the revised baseline winding dimension the clear space between the winding cavities where the centers of the major lobes about one another is reduced to 13 cm. This is judged to be the minimum space required for the coil cases and a clearance.

The revised baseline winding dimensions result in a system cost of \$65 million per end cell, compared to a cost of \$63.4 million per end cell for the design using a 0.2 by 0.8-m winding cavity. Cost calculations were not performed for different coil spacing along the machine axis, but it is judged that accommodating the increased winding size by axially spreading the coils would have a greater impact on cost.

Reducing the shield thickness from 15 cm to the 10 cm incorporated in the baseline design results in an integrated heat load of 2.6 kW on the coil with the greatest neutronic heating. This means that the vapor content exiting the coil will be 9.4% by volume which is less than the limiting criterion of 10%.

Conclusions

The baseline end-plug magnet system configuration and design satisfies all the requirements for plasma performance and mechanical system integration at near-minimum cost. However, the spacing (13 cm) between the major lobes of the c-shaped coils should be evaluated for overall mechanical support of the fault condition magnetic loads.

References

- [1] W. D. Nelson, J. N. Doggett, J. A. O'Toole, "MFTF- α T Progress Report," Oak Ridge National Laboratory Report, ORNL/FEDC-TM-83/9, (to be published).
- [2] T. A. Kozman, S. T. Wang, J. H. VanSant, et al., "Magnets for the Mirror Fusion Test Facility: Testing of First Yin-Yang and the Design and Development of Other Magnets," IEEE Trans. Magn., vol. MAG-19, p. 859, 1983.
- [3] J. H. VanSant, "MFTF East Yin-Yang Magnet Flow Resistance Measurements," Engineering Note- ENC-82-19, CA, 1982.
- [4] J. H. VanSant, "Thermal Performance of the MFTF Magnets," presented at the Cryogenic Engineering Conference, Colorado Springs, Colorado, August 15, 1983. UCRL-88696, Lawrence Livermore National Laboratory, Livermore, CA, 1983.
- [5] L. R. Turner, "Safety of Superconducting Magnets for Fusion: Thermal Analysis of Large Cryostable Magnets," IEEE Trans. Magn., vol. MAG-17, p. 463, 1981.